Laser metal deposition of TiB/Ti6Al4V composites with first-scale network microstructure

Paul Masekuru Lekoadi[1,2], Monnamme Tlotleng[1,3], Charles Witness Siyasiya[2], and Bathusile Nelisiwe Masina[1,4]

[1]Manufacturing, Photonics Centre, Laser Enabled Manufacturing Group, Council for Scientific and Industrial Research, Pretoria, South Africa

[2]Department of Material Science and Metallurgical Engineering, University of Pretoria, Pretoria, South Africa

[3]Material Science Innovation and Modelling Research Group, North-West University, Mmabatho, South Africa

[4]Department of Mechanical Engineering Science, University of Johannesburg, Johannesburg, South Africa

Corresponding author: Paul Masekuru Lekoadi, Manufacturing, Photonics Centre, Laser Enabled Manufacturing Group, Council for Scientific and Industrial Research, P.O. BOX 395, Pretoria 0001, South Africa; Department of Material Science and Metallurgical Engineering, University of Pretoria, Mineral Science Building, Pretoria 0001, South Africa. Email: PLekoadi@csir.co.za

Abstract

This study investigated the effect of in-situ alloying of Ti6Al4V and TiB_2 during laser metal deposition for microstructure, hardness and tensile properties enhancement. It was found that the addition of TiB_2 at powder feed rates of range 0.1–0.3 rpm resulted in the formation of TiB whiskers with columnar and equiaxed network morphologies, in a lamella α + β matrix. By increasing TiB_2 at 0.4–0.5 rpm, a complete dissolution of the equiaxed and columnar network morphologies were achieved. The dissolution led to a random distribution of formed TiB whiskers, resulting in enhanced hardness and ultimate tensile strength (UTS), with the 0.5 rpm giving the highest hardness and UTS values of 511 ± 13 HV and 1745 MPa, respectively.

Keywords: titanium matrix composite, laser metal deposition, microstructure, mechanical properties

Introduction

Titanium and its alloys find their application in low and medium temperature environments. To improve on their existing limitations, alloying their matrix with hard ceramic materials to form composites known as titanium matrix composites (TMCs) have for a while been considered. Various ceramic materials such as titanium boride (TiB),[1] titanium diboride (TiB_2),[2] titanium carbide (TiC),[3] silicon carbide (SiC),[4] boron carbide (B_4C)[5] and titanium nitride (TiN)[6] and have been explored and most recently graphene nanoplatelets (GNPs) and carbon nanotubes (CNTs) are considered as reinforcements as high-performance TMCs.[7,8]

Generally, TMCs are produced using two processing approaches, namely, ex-situ and in-situ synthesis. Ex-situ processing involves the formation of no new compounds during processing

and therefore, there is no change in both particle size and morphology of the added particles before and after processing, provided there are no external impacts.[9,10] As such, thermodynamically stable ceramics such as TiB, TiC and SiC are added to titanium.[9] On the hand, in-situ processing involves reaction of titanium matrix with additive elements such as boron (B), carbon (C) and nitrogen (N) to form in-situ stable phases or reinforcements.[9] Some common examples of additions used in in-situ synthesis include TiB_2, B_4C and Si_3N_4.

By varying the volume fraction of the alloying ceramics, refined microstructures with enhanced mechanical properties are achieved.[11,12] TMCs with network microstructure have proved to endure superior oxidation resistance by effectively pinning and segmenting the oxide scale.[11] Moreover, the network microstructure can lead to components with higher ultimate tensile strength (UTS), improved plasticity and creep resistance.[5,13–15] In this study, in-situ alloying of Ti6Al4V and TiB_2 at various powder feed rates using direct energy deposition (DED) as processing technique are investigated.

There is a significant amount of scientific research that report on the microstructure and mechanical properties of TMCs manufactured with additive manufacturing (AM). Recently, Fereiduni et al.[5] reported the microstructure and mechanical properties of Ti6Al4V/B_4C cubic samples that were manufactured with SLM, using premixed B_4C/Ti6Al4V as the starting material. Their results showed nano-scaled TiB needles which were homogeneously distributed along the large columnar prior β grains, and dispersed within the martensitic matrix. The latter microstructure was found to exhibit an improved YS, UTS and fracture strain of 1284 MPa, 1850 MPa and 20.6%, respectively. The incorporation of the nano-scaled TiB reinforcements led to the refinement of the martensitic phase and solid solution strengthening effect from the carbon atoms.

Pan et al.,[16] using electron beam melting (EBM) and premixed titanium-titanium boride whiskers (Ti6Al4V/TiBw) powder, reported the formation of quasi-network microstructure that contained nano-sized TiBw which was distributed along the grain boundaries of the TiBw/Ti6Al4V matrix composite. The manufactured TiBw/Ti6Al4V composite had YS, UTS and elongation of 1039 MPa, 1121 MPa and 8.9%, respectively. These results are attributed to both microstructural refinement and load bearing strengthening as a result of nano-sized TiBw that had formed.

Using wire arc AM (WAAM) technique, Wang et al.[17] using Ti6Al4V + boron wires as starting materials, manufactured TiB/Ti6Al4V composite samples that had a refined microstructure and TiB whiskers with cyclic gradient morphology. The authors reported that the microstructure refinement was promoted by the gradient distribution of TiB whiskers which had formed on the β grain boundaries and improved the mechanical properties. The formed TMC had UTS of 1089 MPa which was 17% higher than that of the Ti6Al4V. The high UTS was achieved with compromised elongation (that had decreased) and improved tensile strength (increased).

Niu et al.[18] using LMD and premixed Ti–2Fe–0.1B reported the formation of TiB with a 3D quasi-network structure on Ti–2Fe–0.1B. The highest UTS of 779 MPa was reported and attributed to both grain size strengthening effects. Xue et al.[13] investigated the microstructure

and mechanical properties of TiB/Ti6Al4V samples manufactured with a DED technique commonly known as laser solid forming (LSF). It was reported that an increase in boron (B) content changed the prior *β* grain morphology to short columnar and equiaxed. According to their results, the TiB presented three types of morphologies, namely, equiaxed-like, fine needle-like and hollow hexagonal. The YS and UTS were observed to increase with increasing B content, while elongation decreased.

Finally, Zhang et al.[2] successfully fabricated TiBw/Ti6Al4V composite with direct laser deposition (DLD), using premixed TiB_2/Ti6Al4V powder as the starting material, and reported that the microstructure of the TiBw/Ti6Al4V composite exhibited dendritic and equiaxed TiB with network structures, within the Ti6Al4V matrix. In addition, compressive test results revealed an ultimate compressive strength of 1574 MPa.

The reviewed studies show that manufacturing of TiB/Ti6Al4V with different AM techniques can lead to different microstructural characteristics with different mechanical properties being achieved. However, the reviewed literature is limited on the effects of TiB_2 addition (micro-alloying or bulk addition) on the microstructure and mechanical properties of TiB_2/Ti6Al4V composites produced or synthesised by LMD. This suggests that for the development of best performing TMCs, the understanding of the effect of micro-alloying on microstructural characteristics and room temperature mechanical properties is crucial. This study extensively investigated the effect of micro-in-situ alloying on the microstructure and room temperature mechanical properties of laser in-situ synthesised TiB/Ti6Al4V composite produced using the LMD.

Materials and methods

Materials

A spherical gas atomised Grade 5, pre-alloyed Ti6Al4V powder with particle size distribution (PSD) in the range 50–100 µm (supplied by TLS ECKART TLS GmbH) and TiB_2 powder with PSD in the range 45–100 µm (supplied by Nanografi New Technology) were used during deposition. Scanning electron microscope (SEM) images of the Ti6Al4V and TiB_2 powders together with their corresponding PSD curves are presented in Figure 1, respectively. PSD of the powders was conducted using Microtrac Total Solution particle characterisation instrument (CSIR). The powders were deposited on a Ti6Al4V base plate with dimensions 100 mm × 100 mm × 6 mm. The base plate was sandblasted before deposition.

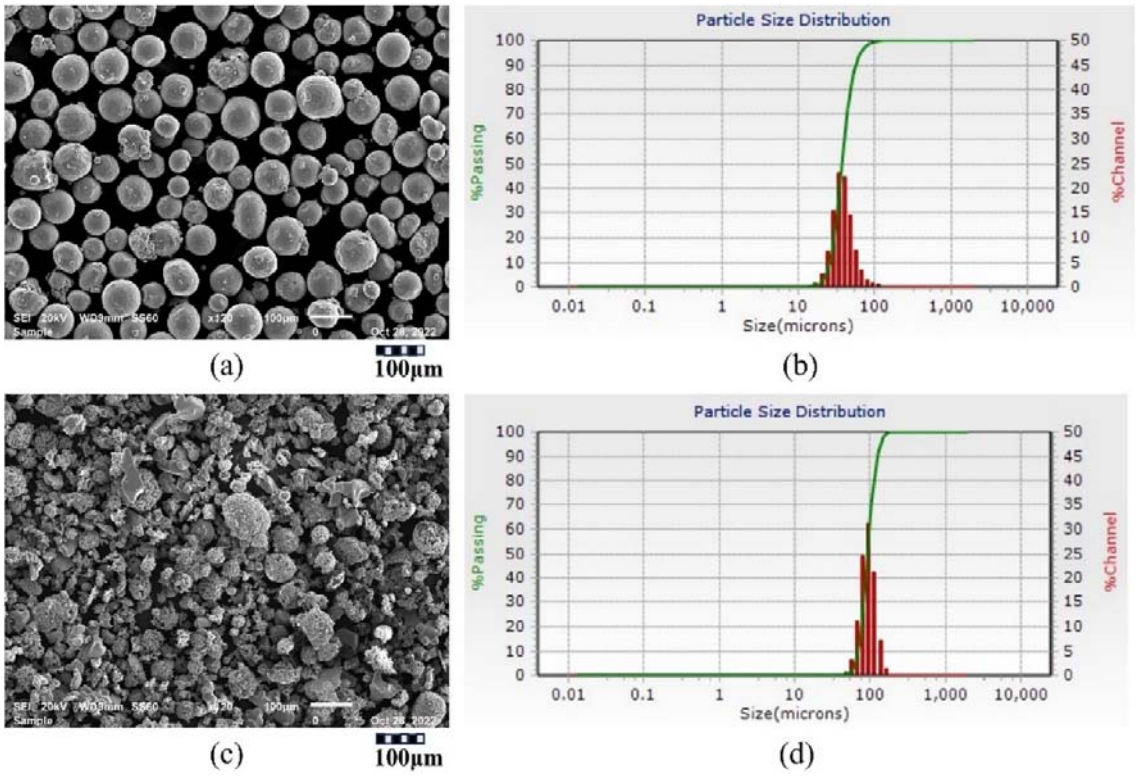

Figure 1. SEM images and PSD curves of the powders, (a) Ti6Al4V, (b) Ti6Al4V PSD, (c) TiB_2 and (d) TiB_2 PSD.

Figure 1(a) shows that Ti6Al4V particles were highly spherical and smooth, with PSD in the range of 26–65 µm as depicted in Figure 1(b). In contrast, the TiB_2 particles presented a mixture of spherical and irregular shapes as can be seen in Figure 1(c), with PSD in the range of 70–132 µm as shown in Figure 1(d).

Methods

Cubic samples of 20 mm × 20 mm × 20 mm dimension were manufactured on a LMD AM machine that is equipped with IPG fibre laser of 1073 nm wavelength. A schematic diagram of the LMD process is depicted in Figure 2. The processing system had a KUKA robot arm onto which the three-way brass nozzle was attached for sample printing. A GTV powder system (D-57629), equipped with two powder feeding hoppers and a controller to deliver independently Ti6Al4V and TiB_2 to the deposition plate through an argon gas as a carrier gas during deposition. During the in-situ alloying, both Ti6Al4V and TiB_2 were simultaneously fed into a laser melt pool whereby Ti6Al4V was deposited at a constant mass feed rate, while TiB_2 powder was deposited at varying powder feed rates given in Table 1.

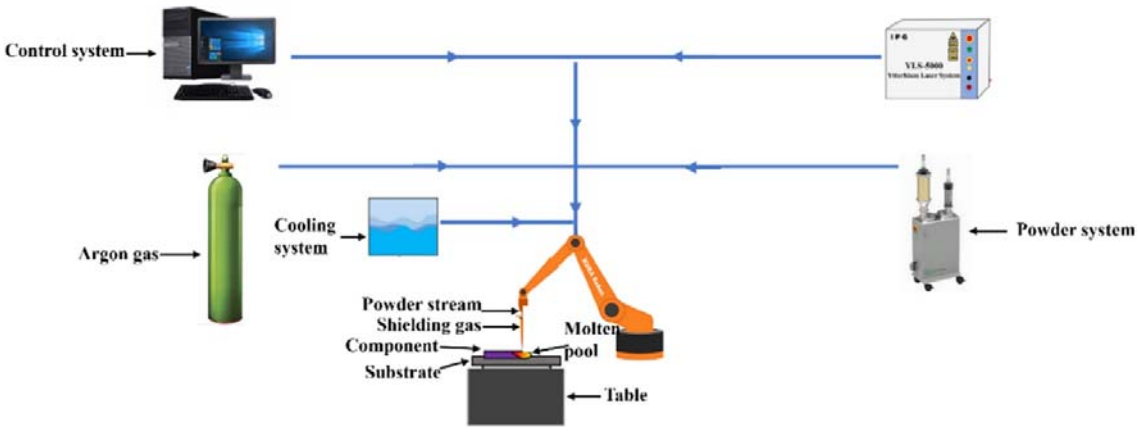

Figure 2. Schematic diagram of LMD process.

Table 1. Powder feed rates.

Sample name	Powder feed rate (rpm)	Percentage powder feed rate (%)
Ti6Al4V	0	0
TMC-1	0.1	1
TMC-2	0.2	2.83
TMC-3	0.3	3.5
TMC-4	0.4	4.8
TMC-5	0.5	6.3

The powder carrier gas was set at 1.5 L/min during the deposition of all samples. Argon gas was used as a protective gas, at gas flow rate of 12 L/min to prevent the samples from oxidising. During the deposition of all the samples, optimised process parameters for laser power, scanning speed and beam diameter were used. Once produced, the samples were then allowed to cool to room temperature before they were prepared for metallographic observations, chemical analyses and mechanical performance.

Metallographic preparations and characterisation

The sample were metallographically prepared using standard grinding and polishing procedures,[1] and were etched with Kroll's reagent, a solution containing 100 mL H_2O, 1–3 mL HF and 2–6 mL HNO_3. The metallographically prepared and etched samples were observed for microstructure using a JOEL JSM-6010PLUS/LA SEM at various magnifications. Phase analysis was conducted using PANalytical X'part (PRO-Netherlands) X-ray diffraction (XRD) machine. The XRD machine was fitted with Cu Kα (α = 0.154 nm) radiation source.

Mechanical testing

Vickers hardness measurements were conducted using Matsuzawa Seiko Vickers model MHT-1 micro-hardness machine. All measurements were done using a diamond tip indenter, while applying a force of 300 gf and dwell time of 10 s. For all samples, three hardness patterns

were measured, and the average was calculated as the overall hardness of the material. Tensile test measurements were conducted using profilometry-based indentation plastometrex (PIP) (PLX-P-0006) machine. Tensile measurements were conducted using a spherical indenter of 1.0 mm radius, and applying a force of 5566 N. It is important to note that three steps are involved in determining the tensile properties of the TiB/Ti6Al4V samples. First step involves pushing a hard indenter into the samples with a force of 5566 N, second step is measuring the radially symmetric profile of the indent, and the third step is iterative simulation of the test until the best fit set of true stress–true strain plasticity parameter values are obtained.[19]

Results and discussions

Microstructure

The SEM micrographs of the TiB/Ti6Al4V samples at various mass flow rates are given in Figure 3. As seen from Figure 3(a), the microstructure of the sample at powder feed rate of 0 rpm presented large columnar prior β grains. Inside the β grains, a fully martensitic α'-structure was presented as shown in Figure 3(a). It must be noted that the martensite α'-phase presented two types of morphologies, namely thinner and thicker laths (Figure 3(a)). It is well-known that the martensite α'-phase forms because of phase transformation from primary β-phase during cooling and solidification of the sample as a result of high cooling rates, associated with LMD process.[14] The same type of martensitic α' microstructure is reported in literature on Ti6Al4V samples manufactured with laser AM techniques.[19–21]

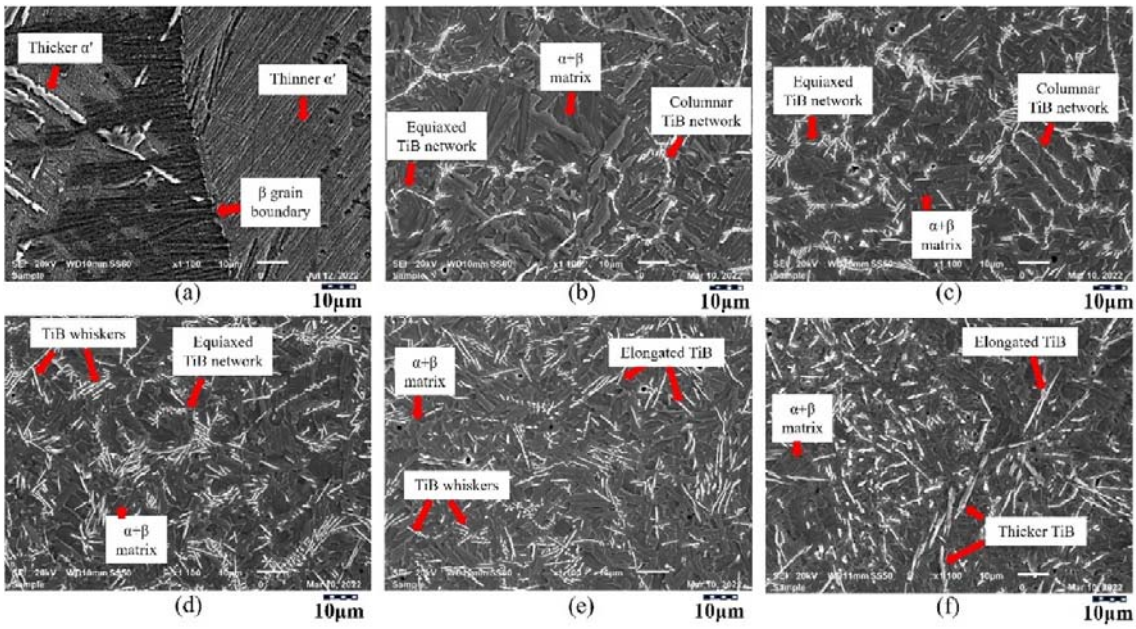

Figure 3. SEM micrographs of the TiB/Ti6Al4V samples at various TiB_2 mass flow rates, (a) 0 rpm, (b) 0.1 rpm, (c) 0.2 rpm, (d) 0.3 rpm, (e) 0.4 rpm and (f) 0.5 rpm.

Figure 3(b) shows that the powder feed rate of TiB_2 at 0.1 rpm resulted in a major microstructural change. Firstly, the matrix was changed from martensitic α' to fully lamella α + β, suggesting slow cooling during the solidification process.[18,22] In other words, the Ti6Al4V matrix was refined by the addition of TiB_2. Secondly, the microstructure of the latter sample consisted of weakly connected in-situ synthesised TiB whiskers with columnar and equiaxed morphology, distributed within the lamella α + β matrix as shown in Figure 3(b). The weak connection of the TiB whiskers was attributed to the lower TiB_2 deposition volume of 1%.[9] Moreover, the formation of the TiB was attributed to the in-situ reaction between the molten Ti6Al4V and TiB_2 during the LMD process according to reaction (1).[23]

$$\mathrm{Ti} + \mathrm{TiB_2} \rightarrow 2\,\mathrm{TiB} \tag{1}$$

According to the literature, the Gibbs free energy (Δ*G*) of formation for reaction (1) is −10 kcal/mol, from which the negative sign clearly indicates spontaneous reaction for the formation of TiB.[2,20] Figure 3(b) shows that the formation of the TiB occurred at the grain boundaries of the parent β-Ti grains. According to Pan et al.,[16] the formation of TiB at the β-Ti grain boundaries is due to boron (B) rich layers around β-Ti nuclei in the meltpool, which result in TiB precipitation and gradual accumulation along β-Ti grain boundaries. In contrast, Dolgun et al.[21] reported that the TiB whiskers are preferably formed on the boundaries of the β-Ti due to high surface tension created by the steep thermal gradient between the edges of the molten pool.

Figure 3(c) shows that by increasing the powder feed rate of TiB_2 to 0.2 rpm resulted in a noticeable grain size decrease of the TiB networks. The grain size decrease was obviously associated with the increased volume of TiB_2, which promoted the formation of more TiB whiskers, and resulted in a slight increase in the number of columnar and equiaxed TiB networks in the lamella α + β matrix. At the same time, the connection of the network TiB was becoming clear, with the formation of shorter and longer needle-like TiB whiskers becoming defined (Figure 3(c)). This observation might be due to the increase in the amount of boron in the titanium matrix. According to Huang et al.,[15] the size of the TiB whiskers together with their spatial distribution is directly related to the mechanical properties. Moreover, the TiB network morphology is known to exhibit improved ductility and high temperature durability by prohibiting grain boundary softening.[15] It is obvious from Figure 3(d) that a further increase of the mass flow rate to 0.3 rpm resulted in an increase in the number of the formed short and needle-like TiB whiskers, while the matrix remained lamella α + β. Furthermore, increasing the powder feed rate to 0.3 rpm resulted in a random distribution and length increase of the TiB whiskers as can be seen in Figure 3(d). Due to the higher amount of TiB_2, the random distribution of the TiB whiskers promoted the dissolution of the columnar and equiaxed network morphologies. In other words, the formation of the TiB whiskers at the β-Ti grain boundaries was becoming undefined.

Figure 3(e) clearly shows that increasing the powder feed rate to 0.4 rpm resulted in the complete spreading of the formed TiB whiskers. This implies a complete dissolution of the columnar and equiaxed network structures. In addition, the length of the TiB whiskers was further increased. More precisely, it was observed from Figure 3(e) that some of the formed

TiB whiskers were connecting to form a more defined and elongated morphology. The formed long TiB whiskers were longer than the samples deposited at powder feed rates of 0.1, 0.2 and 0.3 rpm (Figure 3). It is important to note that the matrix remained lamella α + β regardless of the change in the TiB characteristics. However, the sizes of the lamella α + β phases were slightly decreased as can be seen in Figure 3(e). The decrease in the lamella α + β phases was attributed to the formation of TiB which is known to inhibit the matrix grain growth.[24] It is obvious from Figure 3(f) that increasing the powder feed rate to 0.5 rpm promoted an increase in the size and thickness of the formed TiB whiskers. The increase in size and thickness was followed by a decrease in the size of the matrix lamella α + β phases. It is understood that the random distribution together with the increase in size and thickness was due to the high amount of TiB_2 present in the titanium matrix. In addition, the microstructure of the sample deposited at 0.5 rpm showed two types of TiB whiskers, namely, elongated TiB and short thicker TiB as shown in Figure 3(f).

The microstructure of the sample deposited at a powder feed rate of 0 rpm TiB_2 presented large grained β-grains with martensitic α' phase (Figure 3(a)). The addition of TiB_2 at 0.1 rpm to the titanium bulk matrix transformed the microstructure by forming TiB whiskers on the grain boundaries of the parent β grains, which resulted in a major refinement of the β grains into smaller equiaxed and columnar morphologies (Figure 3(b)). An increase in powder feed rate to 0.2 rpm decreased the size of the equiaxed and columnar β grains and promoted the formation of more defined TiB whiskers. Moreover, 0.2 rpm resulted in a noticeable decrease in the size of the lamella α + β phases of the matrix. A slight increase in random distribution of the TiB whiskers was observed when the powder feed rate was increased to 0.3 rpm, with their length noticeably increasing (Figure 3(d)). The addition of TiB_2 at a powder feed rate of 0.4 rpm resulted in the complete dissolution of the equiaxed and columnar grains and promoted random distribution of the TiB whiskers. While the random distribution of the TiB whiskers was increased when the powder feed rate was increased to 0.5 rpm, their size and length were also increased which promoted further size decrease of the lamella α + β phase of the matrix. For further analysis of the samples, the phase identification using XRD was conducted, and the results are presented next.

Phase identification

XRD patterns showing the phases for Ti6Al4V and TMC samples at various powder feed rates are reported in Figure 4. Figure 4(a) shows that the sample deposited at 0 rpm presented only the martensite α'-Ti phase. This observation supports the microstructure observation where a fully martensitic structure was observed for the Ti6Al4V sample (Figure 3(a)). In contrast, the sample deposited at a powder feed rate of 0.1 rpm showed the presence of three phases, namely, α-Ti, β-Ti and TiB. It must be noted that no TiB_2 peak was observed, implying the occurrence of an in-situ reaction between the molten Ti6Al4V and TiB_2. Figure 4(b) revealed that the addition of TiB_2 at 0.1 rpm resulted in the introduction of the β-Ti phase with planar (1 0 1) at 2ϑ value of 40.85° and TiB phases for planar peaks (2 0 1), (1 1 1) and (2 1 0) at 2ϑ value of 35.78°, 38.83° and 42.79°, respectively. Moreover, deposition at 0.1 rpm was followed by a noticeable improvement in all the diffraction peaks (Figure 4(b)). The improvement in diffraction peaks was attributed to the addition of TiB_2. All the diffraction

peaks dropped when the powder feed rate was increased to 0.2 rpm. The drop in diffraction peaks might be due to the in-situ reaction reaching its saturation point. In addition, the β-Ti phase (1 0 1) at 2ϑ value of 40.85° disappeared when the powder feed rate was increased to 0.2 rpm. However, an additional TiB phase with planar (2 0 1) was observed at a 2ϑ value of 54.27°. Interestingly, all the diffraction peaks were prominently increased when the powder feed rate was increased to 0.3 rpm, with the β-Ti peak (1 0 1) at 40.85° observed as depicted in Figure 4(d). Increasing the powder feed rate to 0.4 rpm resulted in a noticeable decrease in all the diffraction peaks, followed by a slight improvement of the β-Ti peak (1 0 1) at 2ϑ value of 40.85°. A further increase of the powder feed rate to 0.5 rpm resulted in the most increase in all the phase peaks, while the TiB peak at (2 0 1) disappeared. This observation was associated with the higher amount of TiB_2 in the titanium matrix.

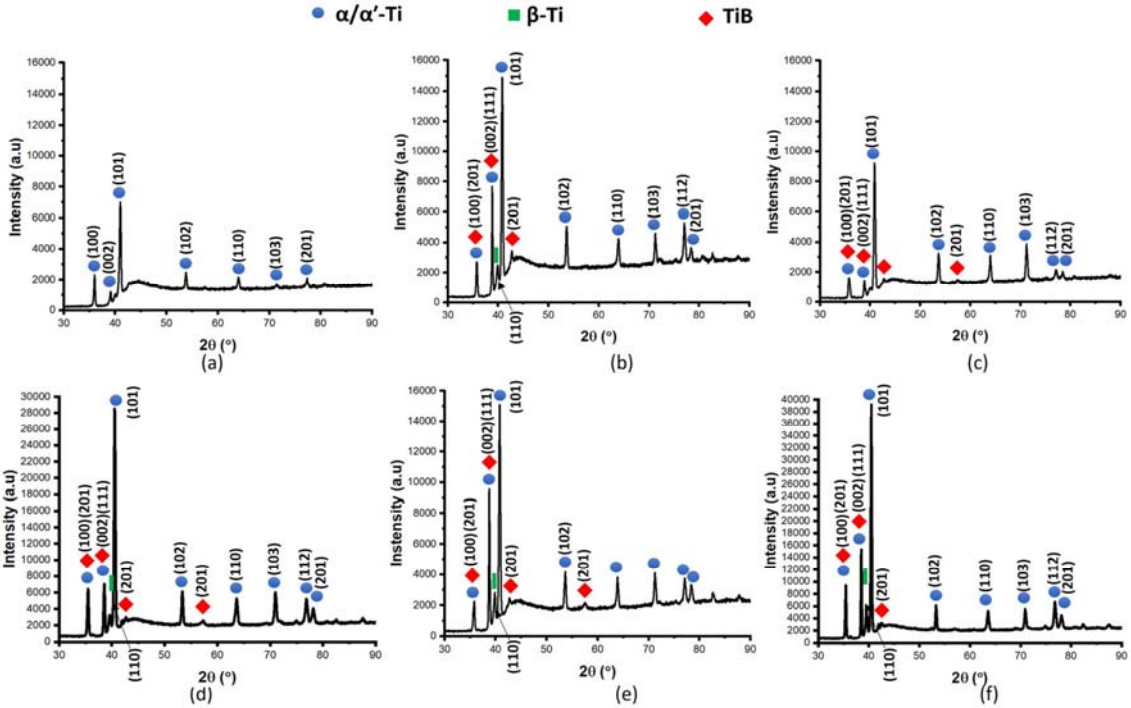

Figure 4. XRD patterns of the TiB/Ti6Al4V at various TiB_2 mass flow rates, (a) 0%, (b) 0.1 rpm, (c) 0.2 rpm, (d) 0.3 rpm, (e) 0.4 rpm and (f) 0.5 rpm.

Hardness

The average hardness profile and values of the TiB/Ti6Al4V sample are presented in Figure 5 and Table 2, respectively. Both Figure 5 and Table 2 show that the sample deposited at 0 rpm gave the lowest hardness profile and average hardness value of 400 ± 15 HV. It was obvious that the low hardness was associated with the fully martensitic α' microstructure that was observed in Figure 3(a).[21,25] The hardness was remarkably increased to 474 ± 10 HV when TiB_2 was added at 0.1 rpm to the Ti6Al4V. The increase in hardness was attributed to the formation of hard TiB whiskers[19,26] in the titanium matrix as observed on the microstructure in Figure 3(a). According to the literature, the increase in hardness promoted by the formation of the TiB can generally lead to improved wear resistance and stiffness.[26,27]

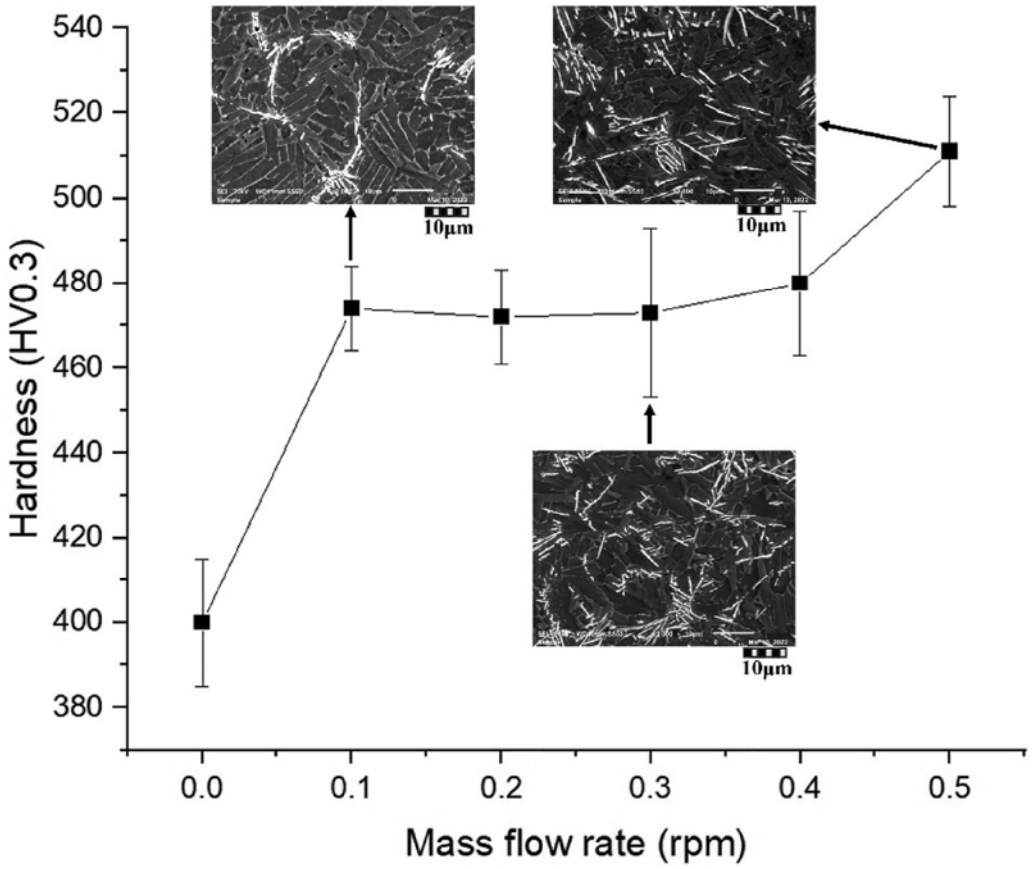

Figure 5. Average hardness profile of the TiB/Ti6Al4V at various mass flow rates.

Table 2. Average hardness of the TiB/Ti6Al4V.

Sample	**$HV_{0.3}$**
0 rpm	400 ± 15
0.1 rpm	474 ± 10
0.2 rpm	472 ± 11
0.3 rpm	473 ± 20
0.4 rpm	480 ± 17
0.5 rpm	511 ± 13

Table 2 further shows that increasing the powder feed rates to 0.2 rpm and 0.3 rpm did not initiate any major change in hardness since the hardness values of the latter samples were quite similar. The similarity in hardness values was attributed to the similar microstructural characteristic whereby equiaxed and columnar TiB grains were observed in lamella α + β matrix (Figure 3(b)–(d)). A slight increase in hardness to 480 ± 17 HV was observed when the powder feed rate was increased to 0.4 rpm. The slight hardness increase was attributed to the random distribution of the TiB whiskers that promoted grain refinement of the matrix's lamella α + β phases and dissolution of the equiaxed and columnar grains according to the Hall–Petch relationship given in equation (2).[28]

$$\mathrm{HV} = \mathrm{HV}_0 + \frac{ky}{\sqrt{d}} \quad (2)$$

where HV is the hardness, *d* is the grain size, HV_0 and *ky* are the material constants representing the hardness of a grain-free material and the hardening coefficient, respectively. Therefore, smaller grains will result in increased hardness. A noticeable increase in hardness to 511 ± 13 HV was observed when the powder feed rate was increased to 0.5 rpm as presented in Figure 5 and Table 2. It was obvious that the increase in hardness was attributed to random distribution and an increase in the size of the TiB whiskers which was promoted by the high volume of TiB_2 (Figure 3(f)).

Profilometry-based inverse indentation plastometry (PIP)

Figures 6 and 7 and Table 3 give representatives of the nominal stress–strain curves, graphs of tensile strengths and a summary of the tensile properties for the TiB/Ti6Al4V samples at various powder feed rates. The sample deposited at 0 rpm achieved the lowest yield strength (YS) and UTS of 988 ± 16 MPa and 1092 ± 12 MPa, respectively, as presented in Figure 7 and Table 2. It is obvious that the low strength was associated with the unreinforced microstructure. The results were comparable to those of Keist et al.,[29] who reported YS and UTS of 961 ± 40 MPa and 1072 ± 33 MPa, respectively, on Ti6Al4V samples manufactured with LMD. Both the YS and UTS were significantly increased to 1315 ± 42 MPa and 1510 ± 21 MPa when the TiB_2 was added at a powder feed rate of 0.1 rpm. The increase in strength was attributed to the formation of connected equiaxed and columnar TiB whiskers.[2,15,16] This implies that the introduction of TiB_2 strengthened the titanium matrix. It is important to note that the sample deposited at a powder feed rate of 0.1 rpm gave the highest YS compared to all the other samples. Increasing the powder feed rate to 0.2 rpm resulted in a further increase in UTS to 1602 ± 25 MPa. However, the YS was decreased to 1213 ± 54 MPa. The increase in UTS might be due to the formation of more defined TiB whiskers observed on the microstructure in Figure 3(b). Moreover, the 0.1 rpm sample achieved similar elongation to the Ti6Al4V sample as presented in Figure 6.

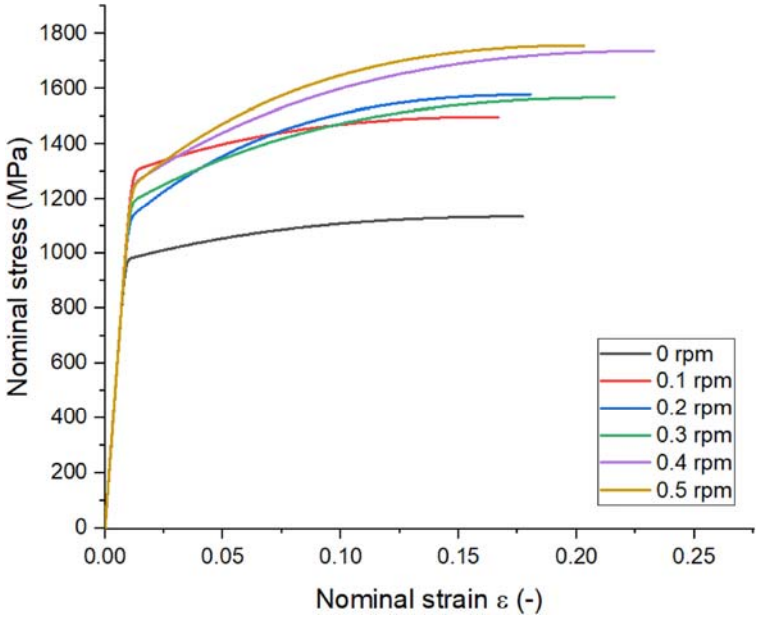

Figure 6. A plot of nominal stress versus strain curves of the Ti6Al4V and TMCs samples up to necking.

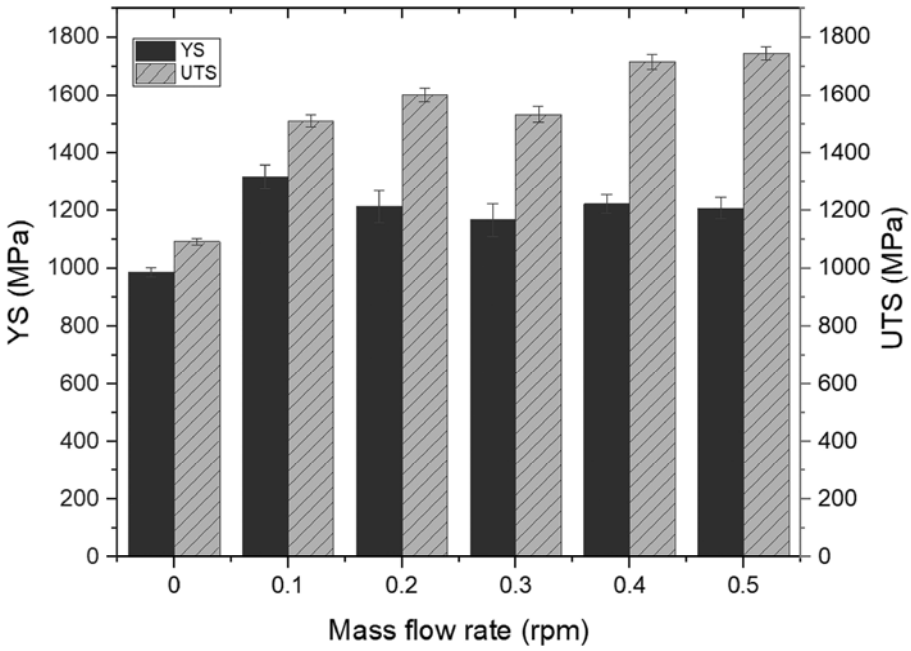

Figure 7. Graphs of the profilometry-based YS and UTS versus mass flow rate.

Table 3. Profilometry-based tensile properties of the Ti6Al4V and TMCs samples.

Mass flow rate	YS (MPa)	UTS (MPa)
0 rpm	988 ± 16	1092 ± 12
0.1 rpm	1315 ± 42	1510 ± 21
0.2 rpm	1213 ± 54	1602 ± 25
0.3 rpm	1166 ± 56	1533 ± 28
0.4 rpm	1222 ± 32	1716 ± 25
0.5 rpm	1207 ± 37	1745 ± 24

A noticeable decrease in both YS and UTS was observed when the powder feed rate was increased to 0.3 rpm as presented in Figure 7 and Table 2. The decrease in strength was attributed to the slight dissolution of the columnar and equiaxed grains (Figure 3(d)) which promoted some random distribution of the TiB whiskers (Figure 3(d)). Moreover, the decrease in strength was followed by an increase in elongation as can be seen in Figure 6. Increasing of TiB_2 powder feed rate to 0.4 rpm resulted in a noticeable increase in both YS and UTS to 1222 ± 32 MPa and 1716 ± 25 MPa, respectively, with elongation also increasing prominently. In fact, the 0.4 rpm sample gave the highest elongation as compared to the other TMC samples. This major increase in strength was attributed to both the matrix grain size decrease (lamella α + β phases) and the size and length increase of the TiB whiskers (Figure 4(e)).[15,28] According to the Hall–Petch equation, the relationship between grain size (*d*) and YS (*σ*) can be given in equation (3).

$$\sigma = \sigma_0 + \frac{ky}{\sqrt{d}} \tag{3}$$

where σ_0 and *ky* are material constants representing the YS of a grain-free material and strengthening coefficient, respectively. Therefore, smaller grain sizes will effectively strengthen the material by blocking dislocation motion.[28] Figure 7 and Table 2 further show that increasing the powder feed rate to 0.5 rpm resulted in an increase in UTS to 1745 ± 25 MPa, at a slight decrease in YS. The above reason accounts for this observation. It must be noted that the 0.5 rpm sample gave the highest UTS value attributed to Hall–Petch strengthening. Moreover, Huang et al.[30] reported that TMCs with the random distribution of the reinforcements exhibit strength enhancement but are accompanied by serous high temperature brittleness.

The deposition of TiB_2 at varying powder feed rates into the bulk matrix of Ti6Al4V plays an important role in the solidification history of the molten pool during LMD, which mainly impacts the microstructure evolution and resulting mechanical properties in hardness, YS and UTS. As can be seen from the results, depositing Ti6Al4V without the addition of TiB_2 with LMD results in a columnar β grained microstructure, with fully martensitic α'-phase as shown in Figure 3(a) due to high cooling and solidification rates in the range 10^3 to 10^6 K/s,[20,31] which was characterised by the lowest hardness, YS and UTS of 400 ± 15 HV, 988 ± 16 MPa and 1092 ± 12 MPa, respectively. The martensite α'-phase is transformed from the full β-phase through a diffusionless process upon cooling of the sample during LMD.[32] Moreover, the martensite α' microstructure is not suitable for applications in medium and high temperature environments due to its metastable nature and microstructural anisotropy promoted by columnar β grains.[17,26] Introducing smaller amounts of TiB_2 into Ti6Al4V matrix (0.1, 0.2 and 0.3 rpm) leads to the formation of in-situ synthesised TiB reinforcements (reaction 1) on the grain boundaries of the β-phase, with refined equiaxed and columnar network distribution (Figure 3(b) and (c)) in a lamella α + β matrix, whereas adding higher amounts (0.4 and 0.5 rpm) result in random distribution of the TiB whiskers, with their length and size increasing with the powder feed rate of TiB_2. The solidification path for the formation of formed TiB

whisker in the lamella α + β matrix during LMD is demonstrated by the TiB pseudo-binary phase diagram presented in Figure 8.

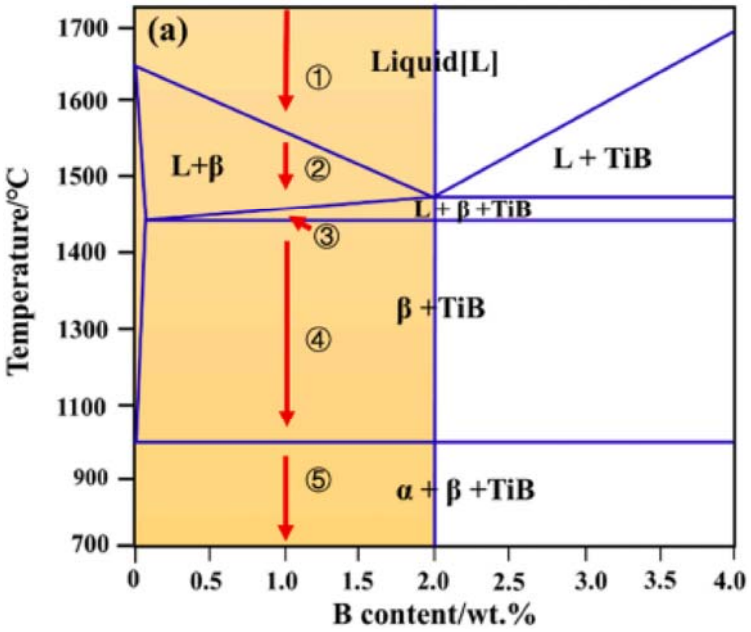

Figure 8. Pseudo-binary phase diagram of TiB.[17]

The XRD results in Figure 4 showed the presence of martensite α' phase on the 0-rpm sample and three phases (α-Ti, β-Ti, TiB) after the addition of TiB_2, irrespective of the powder feed rate. The formation of these phases follows the same solidification path as shown in Figure 8 (Liquid → Liquid + primary β-Ti → β-Ti + TiB → α-Ti + β-Ti + TiB). In other words, both the Ti6Al4V and TiB_2 powder are melted during LMD and solidify into α-Ti, β-Ti and TiB upon cooling. However, the morphology, size and distribution characteristics of the TiB are determined by the added amount of TiB_2. For example, the microstructures of the samples deposited at lower powder feed rates (0,1, 0.2 and 0.3 rpm) formed connected TiB whiskers at the defined columnar and equiaxed β grain boundaries, with the β grain size decreasing with increasing powder feed rate. As explained in Section 'Microstructure,' the formation of TiB on the β grain boundaries was promoted by both TiB rich liquid and β-phase growth that transforms into β + TiB during solidification, through eutectic reaction, leading to the β grain surrounded by TiB whiskers,[33] leading to increased hardness, YS and UTS as presented by Figures 5 and 7 and Tables 2 and 3. The increase in the respective mechanical properties is associated with the formation of in-situ TiB whiskers together and equiaxed and columnar grain morphology. Meanwhile, a decrease in grain size of these columnar and equiaxed networks was observed when the powder feed rate was increased to 0.2 rpm, but the matrix remained lamella α + β (Figures 4(b) and (c)). According to Fereiduni et al.,[26] the formed TiB whiskers are considered highly stable in titanium matrix and cause restricted grain boundary movement and further act as strong barriers for mobile dislocations, leading to improved high temperature performance.

On the contrary, increasing the powder feed rates to higher values of 0.4 and 0.5 rpm results in the complete dissolution of the equiaxed and columnar β grains, promoting the random

distribution of the TiB whiskers (Figures 3(e)–(g)) with greatly enhanced hardness, YS and UTS. In fact, the sample that was deposited with the highest powder feed rate of 0.5 rpm gave the highest hardness and UTS of 511 ± 13 HV and 1745 ± 24 MPa, respectively. It is worth mentioning that the size and length of the TiB whiskers increased with increasing deposition volume, which resulted in a decrease in the sizes of the matrix lamella α + β phases (Figure 4). The growth in length and size resulted from the connection between the smaller and bigger TiB whiskers promoted by the high amount of boron in the titanium matrix following the Ostwald Ripening mechanism, which states that larger TiB needles get bigger at the expense of smaller ones.[34] Fereiduni et al.[26] reported that the formation of bigger TiB whiskers plays an important role in the improvement of creep performance. Wang et al.[17] reported that random distribution of the TiB whiskers promotes excellent tensile properties on TiB/Ti6Al4V composite.

Conclusion

In this work, cubic in-situ synthesised TiB/Ti6Al4V composites were manufactured with LMD technique and the effects of adding TiB_2 into Ti6Al4V matrix on microstructure, hardness and tensile properties were investigated. The following conclusions are drawn:

- The addition of a smaller amount of TiB_2 into Ti6Al4V promotes the formation of TiB reinforcements equiaxed and columnar morphologies at the refined β grain boundaries, with enhanced hardness, YS and UTS.
- The addition of a higher amount of TiB_2 into Ti6Al4V results in the complete dissolution of the equiaxed and columnar β grains, resulting in a random distribution of the TiB whiskers a microstructure with randomly distributed TiB whiskers with enhanced UTS.
- The size and length of the TiB whiskers and lamella α + β matrix increases with increasing deposition volume.
- The highest powder feed rate of 0.5 rpm gave the largest and longest TiB whiskers and the most enhanced mechanical properties, with hardness, YS and UTS reaching maximum values of 511 ± 13 HV, 1315 ± 42 MPa and 1745 ± 24 MPa.

Acknowledgements

The authors would like to thank the Council for Scientific and Industrial Research (CSIR) for providing laboratory facilities. They also thank the Department of Science and Innovation (DSI) of South Africa through the Collaboration Program in Additive Manufacturing (CPAM), grant number HLM3BMX for funding. A special thanks to Mr Samuel Skhosane from CSIR for helping with laboratory work and Mr Tiaan Pretorius from the University of Pretoria for assisting with PIP measurements.

Declaration of conflicting interests

The authors declared no potential conflicts of interest with respect to the research, authorship, and/or publication of this article.

Funding

The authors disclosed receipt of the following financial support for the research, authorship, and/or publication of this article: This work was supported by the Department of Science and Innovation, South Africa (grant number HLM3BMX).

ORCID iD

Paul Masekuru Lekoadi https://orcid.org/0000-0001-6032-6078

References

1. Lekoadi PM, Tlotleng M, Masina BN. Effect of substrate heating on the microstructure and hardness of TiB/Ti6Al4V-ELI during laser in-situ metal deposition. In: Conference of the South African advanced material initiative.

2. Zhang Q, Sun W, Xu S, et al. Nano TiB whiskers reinforced Ti6Al4V matrix composite fabricated by direct laser deposition: microstructure and mechanical properties. *J Alloys Compd* 2022; 922: 1–12.

3. Wang J, Li L, Lin P,. et al. Effect of TiC particle size on the microstructure and tensile properties of TiCp/Ti6Al4V composite fabricated by laser metal deposition. *Opt Laser Technol* 2018; 105: 195–206.

4. Shivakumar G, Ananthi V, Ramanathan S. Production and mechanical properties of nano SiC particle reinforced Ti6Al4V matrix composite. *Trans Nonferrous Met Soc China* 2017; 27: 82–90.

5. Fereiduni E, Ghasemi A, Elbestawi M. Unique opportunities for microstructure engineering via trace B_4C addition to Ti6Al4V through laser powder bed fusion process: as-built and heat treated scenarios. *Addit Manuf* 2022; 50: 1–19.

6. Gu D, Hong C, Meng G. Densification, microstructure and wear property of in-situ titanium nitride-reinforced titanium silicide matrix composites prepared by a novel selective laser melting process. *Metall Mater Trans A* 2012; 43: 697–708.

7. Yan Q, Chen B, Li JS. Super-high-strength graphene/titanium composite fabricated by selective laser melting. *Carbon* 2021; 174: 451–462.

8. Zhang W, Zhou S, Ren W, et al. Uniformly dispersing GNPs for fabricating graphene reinforced pure Ti matrix composite with enhanced strength and ductility. *J Alloys Compd* 2021; 888: 161527.

9. Hayat DM, Singh H, He Z,. et al. Titanium metal matrix composites: an overview. *Compos Part A Appl Sci Manuf* 2019; 121: 418–438.

10. Kondoh K. Titanium metal matrix composites by powder metallurgy (PM) routes. *Titanium*

11. Wei SL, Huang LJ, Li XT, et al. Interactive effects of cyclic oxidation and structural evolution of Ti6Al4V/(TiC + TiB) alloy composite at elevated temperatures. *J Alloys Compd* 2013; 752: 69–175.

12. Jiao Y, Huang L, Geng L. Progress on discontinuously reinforced titanium matrix composites. *J Alloys Compd* 2018; 767: 1196–1215.

13. Sigh G, Ramamurty U. Boron modified titanium alloys. *Prog Mater Sci* 2020; 111: 1–54.

14. Xue A, Lin X, Wang L, et al. Influence of traces of boron addition on microstructure, tensile properties, and their anisotropy of Ti6Al4V fabricated by laser directed energy deposition. *Mater Des* 2019; 181: 1–15.

15. Huang L, An Q, Geng L. Multiscale architecture and superior high-temperature performance of discontinuously reinforced titanium matrix composites. *Adv Mater* 2021; 33: 1–27.

16. Pan D, Li S, Liu L, et al. Enhanced strength and ductility of nano-TiBw-reinforced titanium matrix composites fabricated by electron beam powder bed fusion using Ti6Al4V–TiBw composite powder. *Addit Manuf* 2022; 50: 1–15.

17. Wang ZW, Fu LQ, Wang SL, et al. Balance of strength and plasticity of additive manufactured Ti6Al4V alloys by forming TiB whiskers with cyclic gradient distribution. *Addit Manuf* 2021; 39: 1–12.

18. Niu J, Dai G, Guo Y, et al. Microstructure and mechanical properties of B modified Ti-Fe alloy manufactured by casting, forging and laser melting deposition. *Compos B: Eng* 2021; 261: 1–10.

19. Sousa BC, Cote DL. Profilometry-based indentation plastometry brings speed and accuracy to metallurgical R&D. *Adv Mater Process* 2022; 19: 19–24.

20. Verma PK, Warghane S, Nichul U, et al. Effect of boron addition on microstructure, hardness and wear performance of Ti6Al4V alloy manufactured by laser powder bed fusion additive manufacturing. *Mater Charact* 2021; 172: 1–11.

21. Dolgun E, Zemlyakov E, Shalnova S, et al. The influence of heat treatment on the microstructure of products manufactured by direct laser deposition using titanium alloy Ti6Al4V. *Mater Today* 2020; 30: 688–693.

22. Lekoadi P, Tlotleng M, Annan K, et al. Evaluation of heat treatment parameters on microstructure and hardness properties of high-speed selective laser melted Ti6Al4V. *Metals* 2021; 255: 1–15.

23. Huang LJ, Geng L, Xue HY, et al. In situ TiC particles Ti6Al4V matrix composite reinforced with a network reinforcement architecture. *Mater Sci Eng A* 2011; 528: 2859–2862.

24. Huang LJ, Geng L, Peng HX. Microstructurally inhomogeneous composites: is a homogeneous distribution optimal? *Prog Mater Sci* 2015; 71: 93–168.

25. Gupta A, Khatirkar RK, Kumar A,. et al. Investigation on the effects of heating temperature and cooling rate on evolution of microstructure in α+β titanium alloys. *Mater Res Soc* 2018; 54: 1–12.

26. Fereiduni E, Ghasemi A, Elbestawi M. Tib reinforced Ti6Al4V matrix composites with improved short-term creep performance fabricated by laser powder bed fusion. *J Manuf Proc* 2021; 70: 593–607.

27. Cai C, He S, Li L, et al. In situ TiB/Ti6Al4V composite with a tailored architecture produced by hot isostatic pressing: microstructure evolution, enhanced tensile properties and strengthening mechanism. *Compos B: Eng* 2019; 164: 546–558.

28. Zuback JS, Debroy T. Hardness of additively manufactured alloys. *Materials* 2018; 11: 2–41.

29. Keist JS, Palmer TA. Development of strength-hardness relationship in additively manufactured titanium alloys. *Mater Sci Eng A* 2017; 693: 214–224.

30. Huang L, Geng L. *Discontinuously reinforced titanium matrix composites*. Harbin: Springer, 2017.

31. Azarniya A, Colera XG, Mirzaali MJ, et al. Additive manufacturing of Ti6Al4V parts through laser metal deposition (LMD): process, microstructure, and mechanical properties. *J Alloys Compd* 2019; 804: 163–191.

32. Liu S, Shin YC. Additive manufacturing of Ti6Al4V alloy: a review. *Mater Des* 2019; 164: 107552.

33. Whang SH. Rapidly solidified titanium alloys for high temperature applications. *J Mater Sci* 1986; 21: 2224–2238.

34. Jeong H, Kim S, Hyun Y,. et al. Densification, and compressive strength of in-situ processed Ti/TiB composites by powder metallurgy. *Met Mater Int* 2002; 8: 25–35.